# Analysis of an Adaptive Observer for Sensorless Control of PMSM Drives

Antti Piippo, Marko Hinkkanen, and Jorma Luomi
Power Electronics Laboratory
Helsinki University of Technology
P.O. Box 3000, FI-02015 TKK, Finland

***Abstract*— The paper deals with a speed and position estimation method for the sensorless control of permanent magnet synchronous motors. The method is based on a speed-adaptive flux observer augmented with a high-frequency signal injection method at low speeds. The dynamics of the adaptive observer are analyzed by linearizing both the motor model and the observer, and the observer gain is selected to give improved damping and noise suppression. The experimental results are in agreement with the results of the analysis.**

## I. Introduction

Vector control of a permanent magnet synchronous motor (PMSM) requires information of the rotor position. In sensorless control, the rotor speed and position are estimated without mechanical sensors. The estimation methods can be classified into two main strategies: fundamental-excitation methods and signal injection methods. Fundamental-excitation methods are based on the dynamic model of the motor. The estimation algorithm can be a voltage model [1], or a more complicated observer can be used [2], [3]. Fundamental-excitation methods have good dynamic properties, but they do not allow sustained operation at low speeds. To overcome this problem, various high-frequency (HF) signal injection methods have been developed [4], [5]; these methods are based on detecting the anisotropy caused by the saliency of the rotor or by magnetic saturation. Signal injection methods are well suited to operation at low speeds, including zero speed, but tend to have limited dynamic performance.

The two different approaches can be combined by using a fundamental-excitation method above a certain speed limit and switching to a signal-injection method at low speeds [6], [7]. It is also possible to couple the methods: a voltage model or an adaptive observer is used in the whole speed range and augmented with a signal injection method at low speeds [8], [9]. In such a combined method, the fundamental-excitation method is responsible for the dynamic performance, and the signal injection method stabilizes the operation in the low-speed range down to zero speed.

In this paper, the dynamic properties of the adaptive observer used in [9] are investigated. A linearized model is derived for the observer and the PMSM. Based on the analysis, a feedback gain is selected for the observer, improving the dynamic properties of the system. Finally, experimental results are presented.

## II. PMSM Model

The PMSM is modeled in the $d$-$q$ reference frame fixed to the rotor. The $d$ axis is oriented along the permanent magnet flux, whose angle in the stator reference frame is $\theta_m$ in electrical radians. The stator voltage equation is

$$\mathbf{u}_s = R_s\mathbf{i}_s + \dot{\boldsymbol{\psi}}_s + \omega_m\mathbf{J}\boldsymbol{\psi}_s \tag{1}$$

where $\mathbf{u}_s = [\,u_d \;\; u_q\,]^T$ is the stator voltage, $\mathbf{i}_s = [\,i_d \;\; i_q\,]^T$ the stator current, $\boldsymbol{\psi}_s = [\,\psi_d \;\; \psi_q\,]^T$ the stator flux, $R_s$ the stator resistance, $\omega_m = \dot{\theta}_m$ the electrical angular speed of the rotor, and

$$\mathbf{J} = \begin{bmatrix} 0 & -1 \\ 1 & 0 \end{bmatrix}$$

The stator flux is

$$\boldsymbol{\psi}_s = \mathbf{L}\mathbf{i}_s + \boldsymbol{\psi}_{pm} \tag{2}$$

where $\boldsymbol{\psi}_{pm} = [\,\psi_{pm} \;\; 0\,]^T$ is the permanent magnet flux and

$$\mathbf{L} = \begin{bmatrix} L_d & 0 \\ 0 & L_q \end{bmatrix}$$

is the inductance matrix, $L_d$ and $L_q$ being the direct- and quadrature-axis inductances, respectively. The electromagnetic torque is given by

$$T_e = \frac{3p}{2}\boldsymbol{\psi}_s^T\mathbf{J}^T\mathbf{i}_s \tag{3}$$

where $p$ is the number of pole pairs.

## III. Observer Structure

### A. Adaptive Observer

In an adaptive observer, the rotor speed and position estimation is based on the estimation error between two different models (a reference model and an adaptive model) [10], [11]. The estimated variable can be, e.g., the stator flux or the stator current. An error term is constructed from the two estimates, and used in an adaptation mechanism. The output of the adaptation mechanism, usually the rotor speed or position, is fed back to the adaptive model.

In the following, the stator flux is estimated with two models, and the estimate of the rotor speed is used for adjusting the adaptive model. The block diagram of the adaptive observer is shown in Fig. 1. The observer is formulated in the estimated rotor reference frame. The reference model is based on (2); this flux model can be written as

$$\hat{\boldsymbol{\psi}}_{s,i} = \hat{\mathbf{L}}\mathbf{i}_s' + \hat{\boldsymbol{\psi}}_{pm} \tag{4}$$

0-7803-9252-3/05/$20.00 ©2005 IEEE

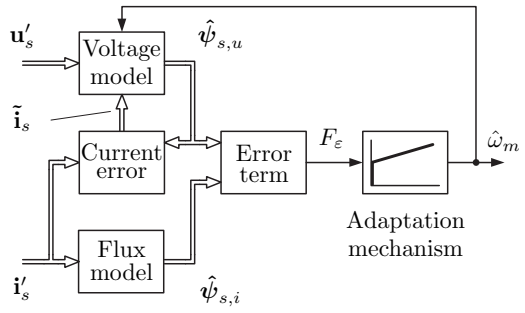


Fig. 1. Block diagram of the adaptive observer.

where estimated quantities are marked by $\hat{}$ and measured quantities expressed in the estimated rotor reference frame are marked by $'$.

The adaptive model is based on (1) and (2). It is here referred to as a voltage model, and defined by

$$\dot{\hat{\boldsymbol{\psi}}}_{s,u} = \mathbf{u}'_s - \hat{R}_s\hat{\mathbf{i}}_s - \hat{\omega}_m\mathbf{J}\hat{\boldsymbol{\psi}}_{s,u} + \boldsymbol{\lambda}\tilde{\mathbf{i}}_s \tag{5}$$

where the estimate of the stator current and the estimation error of the stator current are

$$\hat{\mathbf{i}}_s = \hat{\mathbf{L}}^{-1}(\hat{\boldsymbol{\psi}}_{s,u} - \hat{\boldsymbol{\psi}}_{pm}) \tag{6}$$

$$\tilde{\mathbf{i}}_s = \mathbf{i}'_s - \hat{\mathbf{i}}_s \tag{7}$$

respectively. The feedback gain of the observer is

$$\boldsymbol{\lambda} = \lambda_1\mathbf{I} + \lambda_2\mathbf{J} \tag{8}$$

where $\mathbf{I}$ is the 2-by-2 identity matrix, and $\lambda_1$ and $\lambda_2$ are scalar gain parameters. A pure voltage model is obtained by selecting $\lambda_1 = -\hat{R}_s$ and $\lambda_2 = 0$.

There are various alternatives for obtaining an error term from the flux estimates (4) and (5). In the following, the error term is defined

$$F_\varepsilon = \mathbf{C}_1\tilde{\boldsymbol{\psi}}_s \tag{9}$$

where $\tilde{\boldsymbol{\psi}}_s = \hat{\boldsymbol{\psi}}_{s,i} - \hat{\boldsymbol{\psi}}_{s,u}$ is the difference between the flux estimates, and $\mathbf{C}_1 = [\,0\;\;1\,]$. Hence the flux difference in the estimated $q$ direction is used for adaptation. The estimate of the electrical angular speed of the rotor, used for adaptation in (5), is obtained by a PI speed adaptation mechanism

$$\hat{\omega}_m = -k_pF_\varepsilon - k_i\int F_\varepsilon dt \tag{10}$$

where $k_p$ and $k_i$ are nonnegative gains. The estimate for the rotor position is obtained by integrating $\hat{\omega}_m$.

The gains $k_p$ and $k_i$ of the adaptation mechanism are selected as [9]

$$k_p = \frac{2\alpha_{fo}}{\hat{\psi}_{pm}}, \quad k_i = \frac{\alpha_{fo}^2}{\hat{\psi}_{pm}} \tag{11}$$

where the design parameter $\alpha_{fo}$ corresponds to the approximate bandwidth of the adaptive observer.

### B. Coupling HF Signal Injection to the Adaptive Observer

Since the adaptive observer cannot estimate the rotor speed and position accurately at low speeds due to inaccuracies in measurements and parameter estimates, an HF signal injection method is used to stabilize the observer. The method for coupling the HF signal injection to the adaptive observer has been presented in [9], and is briefly summarized here.

By using the HF signal injection method with an alternating voltage as a carrier excitation signal, an error signal $\varepsilon \approx 2K_\varepsilon\tilde{\theta}_m$ proportional to the position estimation error $\tilde{\theta}_m = \theta_m - \hat{\theta}_m$ is obtained, $K_\varepsilon$ being the signal injection gain. The error signal is used for correcting the estimated position by influencing the direction of the stator flux estimate of the adaptive model. The algorithm is given by

$$\dot{\hat{\boldsymbol{\psi}}}_{s,u} = \mathbf{u}'_s - \hat{R}_s\hat{\mathbf{i}}_s - (\hat{\omega}_m - \omega_\varepsilon)\mathbf{J}\hat{\boldsymbol{\psi}}_{s,u} + \boldsymbol{\lambda}\tilde{\mathbf{i}}_s \tag{12}$$

and

$$\omega_\varepsilon = \gamma_p\varepsilon + \gamma_i\int \varepsilon dt \tag{13}$$

where $\gamma_p$ and $\gamma_i$ are the gains of the PI mechanism driving the error signal $\varepsilon$ to zero. In accordance with [8], these gains are selected as

$$\gamma_p = \frac{\alpha_i}{2K_\varepsilon}, \quad \gamma_i = \frac{\alpha_i^2}{6K_\varepsilon} \tag{14}$$

where $\alpha_i$ is the approximate bandwidth of the PI mechanism. At low speeds, the combined observer relies both on the signal injection method and on the adaptive observer. The influence of the HF signal injection is decreased linearly with increasing speed, reaching zero at transition speed $\omega_\Delta$. At higher speeds, the estimation is based only on the adaptive observer.

## IV. Dynamic Analysis

### A. Linearization

In the following, the focus is on the dynamic properties of the adaptive observer. The dynamics of the flux error are derived, and combined with the speed adaptation mechanism for investigating the stability and damping of the adaptive observer. It is assumed that the estimates of the motor parameters are exact.

The dynamics of the current estimation error (7) are first linearized. For this purpose, both the dynamics of the motor current and the dynamics of the adaptive observer are considered. The result is

$$\begin{aligned}\dot{\tilde{\mathbf{i}}}_s = {} & (-R_s\mathbf{L}^{-1} - \omega_{m0}\mathbf{L}^{-1}\mathbf{J}\mathbf{L} - \mathbf{L}^{-1}\boldsymbol{\lambda})\tilde{\mathbf{i}}_s \\ & + (\mathbf{J}\mathbf{i}_{s0} - \mathbf{L}^{-1}\mathbf{J}\mathbf{L}\mathbf{i}_{s0} - \mathbf{L}^{-1}\mathbf{J}\boldsymbol{\psi}_{pm})\tilde{\omega}_m \\ & + (\omega_{m0}\mathbf{L}^{-1}\mathbf{J}\mathbf{L}\mathbf{J}\mathbf{i}_{s0} + \omega_{m0}\mathbf{i}_{s0} + \omega_{m0}\mathbf{L}^{-1}\boldsymbol{\psi}_{pm})\tilde{\theta}_m\end{aligned} \tag{15}$$

where operating-point quantities are marked by the subscript 0 and $\tilde{\omega}_m = \omega_m - \hat{\omega}_m$ is the speed estimation error. The derivation of (15) is presented in the Appendix.

The dynamics of the flux error are obtained by substituting $\tilde{\mathbf{i}}_s = \mathbf{L}^{-1}\tilde{\boldsymbol{\psi}}_s$ for the current error and $\mathbf{i}_{s0} = \mathbf{L}^{-1}(\boldsymbol{\psi}_{s0} - \boldsymbol{\psi}_{pm})$

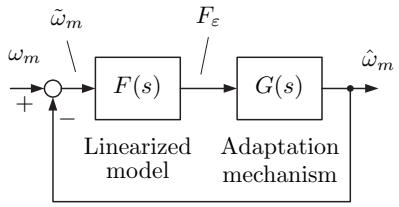


Fig. 2. Block diagram of the linearized model of the adaptive observer.

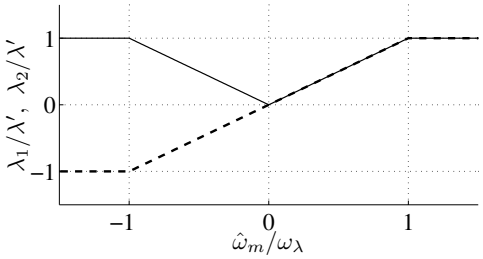


Fig. 3. Observer gain parameters $\lambda_1$ (solid) and $\lambda_2$ (dashed) as a function of the estimated rotor speed.

for the operating-point current in (15):

$$\begin{aligned}\dot{\tilde{\boldsymbol{\psi}}}_s &= \underbrace{(-R_s\mathbf{L}^{-1} - \omega_{m0}\mathbf{J} - \boldsymbol{\lambda}\mathbf{L}^{-1})}_{\mathbf{A}_1}\tilde{\boldsymbol{\psi}}_s \\ &+ \underbrace{(\mathbf{L}\mathbf{J}\mathbf{L}^{-1}(\boldsymbol{\psi}_{s0} - \boldsymbol{\psi}_{pm}) - \mathbf{J}\boldsymbol{\psi}_{s0})}_{\mathbf{B}_1}\tilde{\omega}_m \\ &+ \underbrace{(\omega_{m0}\mathbf{J}\mathbf{L}\mathbf{J}\mathbf{L}^{-1}(\boldsymbol{\psi}_{s0} - \boldsymbol{\psi}_{pm}) + \omega_{m0}\boldsymbol{\psi}_{s0})}_{\mathbf{A}_2}\tilde{\theta}_m\end{aligned} \tag{16}$$

In order to formulate a single-input single-output system, the rotor position error $\tilde{\theta}_m$ is chosen as a state variable in addition to the flux error, and (9) is also used. The resulting state-space representation can be written as

$$\begin{aligned}\begin{bmatrix}\dot{\tilde{\boldsymbol{\psi}}}_s \\ \dot{\tilde{\theta}}_m\end{bmatrix} &= \underbrace{\begin{bmatrix}\mathbf{A}_1 & \mathbf{A}_2 \\ \mathbf{0} & 0\end{bmatrix}}_{\mathbf{A}}\begin{bmatrix}\tilde{\boldsymbol{\psi}}_s \\ \tilde{\theta}_m\end{bmatrix} + \underbrace{\begin{bmatrix}\mathbf{B}_1 \\ 1\end{bmatrix}}_{\mathbf{B}}\tilde{\omega}_m \\ F_\varepsilon &= \underbrace{\begin{bmatrix}\mathbf{C}_1 & 0\end{bmatrix}}_{\mathbf{C}}\begin{bmatrix}\tilde{\boldsymbol{\psi}}_s \\ \tilde{\theta}_m\end{bmatrix}\end{aligned} \tag{17}$$

Hence the transfer function from the speed error $\tilde{\omega}_m(s)$ to the error term $F_\varepsilon(s)$ is given by

$$F(s) = \mathbf{C}(s\mathbf{I} - \mathbf{A})^{-1}\mathbf{B} \tag{18}$$

According to the adaptation mechanism (10), the transfer function from the error term $F_\varepsilon(s)$ to the speed estimate $\hat{\omega}_m(s)$ is

$$G(s) = -k_p - \frac{k_i}{s} \tag{19}$$

Using (18) and (19), the closed-loop system shown in Fig. 2 is obtained. The resulting closed-loop transfer function

$$G_c(s) = \frac{F(s)G(s)}{1 + F(s)G(s)} \tag{20}$$

from $\omega_m(s)$ to $\hat{\omega}_m(s)$ can be evaluated for any operating point.

### *B. Observer Gain Selection*

The observer gain $\boldsymbol{\lambda} = \lambda_1\mathbf{I} + \lambda_2\mathbf{J}$ can be selected in different ways. Using the pole placement design for gain selection is rather complicated due to the fourth-order closed-loop transfer function. A simple alternative is to use zero gain, or to select a constant gain $\lambda_1 > -\hat{R}_s$ and $\lambda_2 = 0$. A negative constant gain was used for PMSM drives in [9]. Better damping can be achieved by a proper selection of $\lambda_1$ and $\lambda_2$. In [12], the speed-dependent gain

$$\lambda_1 = \begin{cases}\lambda'\frac{|\hat{\omega}_m|}{\omega_\lambda}, & |\hat{\omega}_m| \le \omega_\lambda \\ \lambda', & |\hat{\omega}_m| > \omega_\lambda\end{cases} \tag{21a}$$

$$\lambda_2 = \begin{cases}\lambda'\frac{\hat{\omega}_m}{\omega_\lambda}, & |\hat{\omega}_m| \le \omega_\lambda \\ \lambda'\mathrm{sign}(\hat{\omega}_m), & |\hat{\omega}_m| > \omega_\lambda\end{cases} \tag{21b}$$

was used in an adaptive full-order flux observer for induction motor drives. The gain parameters are illustrated in Fig. 3. The positive constants $\lambda'$ and $\omega_\lambda$ can be selected based on the linearized model.

The poles of the closed-loop transfer function $G_c(s)$ were evaluated by using the Control System Toolbox of the MATLAB software. The data given in Section V were used for the motor and for the speed adaptation, and the operating points were defined according to maximum torque per current control [13]. Fig. 4 shows the variation of the poles of $G_c(s)$ for positive nominal torque and varying speed ($-1$ p.u. $\le \omega_{m0} \le$ 1 p.u.). The motor works in the motoring mode at positive speeds and in the regenerating mode at negative speeds.

In Fig. 4, the observer gains are: (a) zero gain; (b) constant gain $\lambda_1 = -0.5\hat{R}_s$ and $\lambda_2 = 0$; (c) speed-dependent gain (21) with $\lambda' = 2\hat{R}_s$ and $\omega_\lambda = 1$ p.u. With the exception of very low speeds, the poles are located in the left half of the complex plane and the linearized system is stable. In the case of the zero gain in Fig. 4(a), one of the upper-half-plane poles shown remains near the imaginary axis but moves far away from the real axis as the speed increases. This pole location indicates insufficient damping at high speeds. In the case of the constant gain in Fig. 4(b), the corresponding pole is closer to the imaginary axis and moves further away from the real axis. The damping is thus even worse than that obtained with zero gain. As the speed-dependent gain is used in Fig. 4(c), the poles move away from the imaginary axis as the speed increases. The damping of the observer is thus improved at higher speeds.

It is worth noticing that different pole locations are obtained at equal speeds in the motoring and regenerating modes of operation. These differences originate from the rotor saliency; the dependence on the load condition disappears if $L_d = L_q$.

At very low speeds (approximately $|\omega_{m0}| < 0.02$ p.u.) in the motoring mode, one of the poles moves to the right half-plane along the real axis for all the feedback gains investigated.

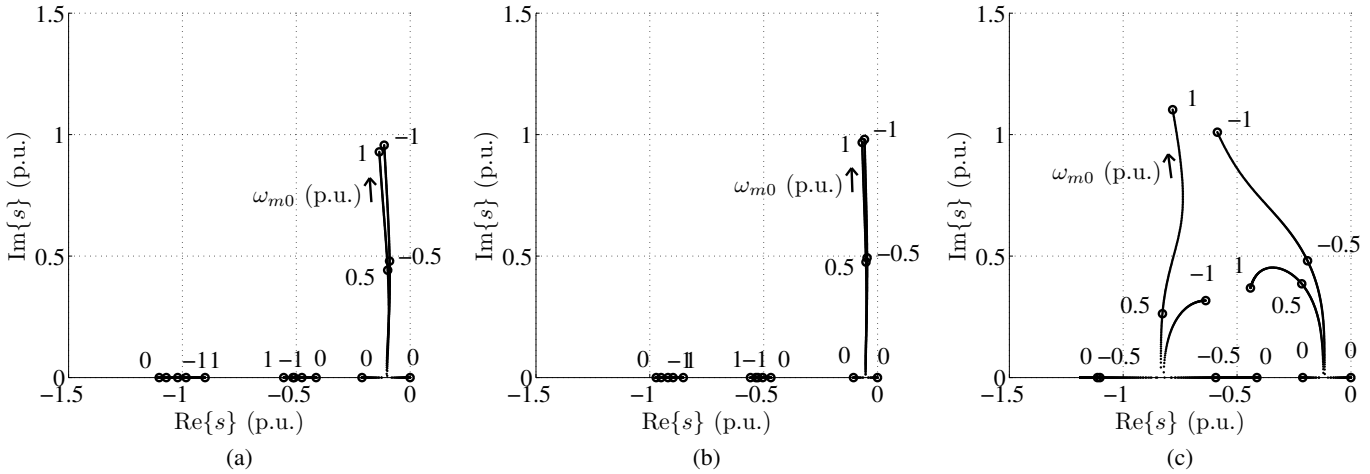


Fig. 4. Variation of poles of $G_c(s)$ at nominal load as rotor speed $\omega_{m0}$ is varied: (a) zero observer gain; (b) constant gain; (c) speed-dependent gain. Due to symmetry, only the upper half-plane is shown.

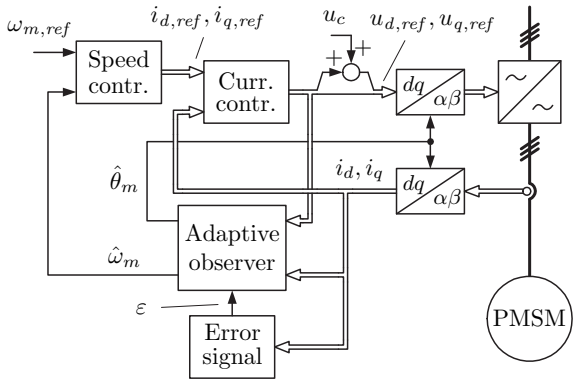


Fig. 5. Block diagram of the control system. Block "Speed contr." includes both the speed controller and the minimization of the current amplitude.

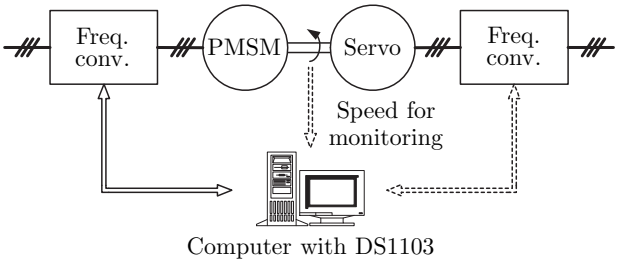


Fig. 6. Experimental setup. Mechanical load is provided by a servo drive.

This phenomenon cannot be seen in Fig. 4 since the pole remains in the close vicinity of the origin. The low-speed instability originates from the rotor saliency; the linearized system is stable (marginally stable at zero speed) in the whole operating region if $L_d = L_q$. The instability of the adaptive observer at very low speeds is not of practical interest; errors in measurements and motor parameters dominate near zero speed in any case. The stability problem is removed by augmenting the observer with the HF signal injection method at low speeds.

TABLE I
MOTOR DATA

| | |
|---|---|
| Nominal power | 2.2 kW |
| Nominal voltage | 370 V |
| Nominal current | 4.3 A |
| Nominal frequency | 75 Hz |
| Nominal speed | 1 500 r/min |
| Nominal torque $T_N$ | 14.0 Nm |
| Number of pole pairs $p$ | 3 |
| Stator resistance $R_s$ | 3.59 Ω |
| Direct-axis inductance $L_d$ | 0.036 H |
| Quadrature-axis inductance $L_q$ | 0.051 H |
| Permanent magnet flux $\psi_{pm}$ | 0.545 Vs |
| Total moment of inertia | 0.015 kgm$^2$ |

TABLE II
CONTROL SYSTEM PARAMETERS

| | |
|---|---|
| Current controller bandwidth | $2\pi$·400 rad/s |
| Speed controller bandwidth | $2\pi$·5 rad/s |
| Speed adaptation bandwidth $\alpha_{fo}$ | $2\pi$·50 rad/s |
| Bandwidth $\alpha_i$ at zero speed | $2\pi$·5 rad/s |

## V. EXPERIMENTAL RESULTS

The different feedback gains of the adaptive observer were investigated by means of simulations and laboratory experiments. The block diagram of the control system comprising cascaded speed and current control loops is shown in Fig. 5. PI-type speed control with active damping is used. The current component references $i_{d,ref}$ and $i_{q,ref}$ are calculated according to maximum torque per current control [13]. The current control is implemented as PI-type control in the estimated rotor reference frame. The dc-link voltage of the converter is measured, and a simple current feedforward compensation for dead times and power device voltage drops is applied [14].

The experimental setup is illustrated in Fig. 6. A six-pole interior-magnet PMSM (2.2 kW, 1500 rpm) is fed by a frequency converter that is controlled by a dSPACE DS1103 PPC/DSP board. The motor data are given in Table I. Mechan-

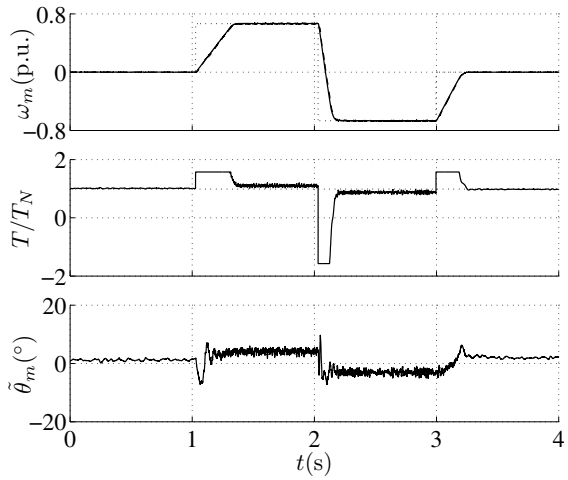


(a)

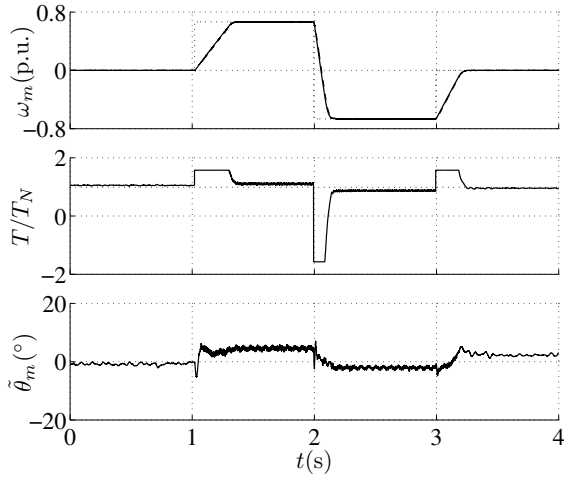


(b)

Fig. 7. Experimental results showing speed reference steps at nominal load torque: (a) constant gain; (b) speed-dependent gain. First subplot shows electrical angular speed (solid), its estimate (dashed), and its reference (dotted). Second subplot shows estimated electromagnetic torque (solid) and load torque reference (dotted). Last subplot shows estimation error of rotor position in electrical degrees.

ical load is provided by a PMSM servo drive. An incremental encoder is used for monitoring the actual rotor speed and position. The nominal dc-link voltage is 540 V, and the switching frequency and the sampling frequency are both 5 kHz. The HF carrier excitation signal has a frequency of 833 Hz and an amplitude of 40 V, and the transition speed $\omega_\Delta = 0.13$ p.u. The electromagnetic torque is limited to 22 Nm, which is 1.57 times the nominal torque $T_N$. Other parameters of the control system are given in Table II.

Fig. 7 shows experimental results obtained at the nominal load torque. The speed reference was first changed stepwise from zero to 0.67 p.u. at $t$ = 1 s, then reversed to $-0.67$ p.u. at $t$ = 2 s, and finally set to zero at $t$ = 3 s. The constant gain $\lambda_1 = -0.5\hat{R}_s$ and $\lambda_2 = 0$ was used in Fig. 7(a), and the speed-dependent gain (21) with $\lambda' = 2\hat{R}_s$ and $\omega_\lambda = 1$ p.u. was used in Fig. 7(b). In both cases, the estimated rotor

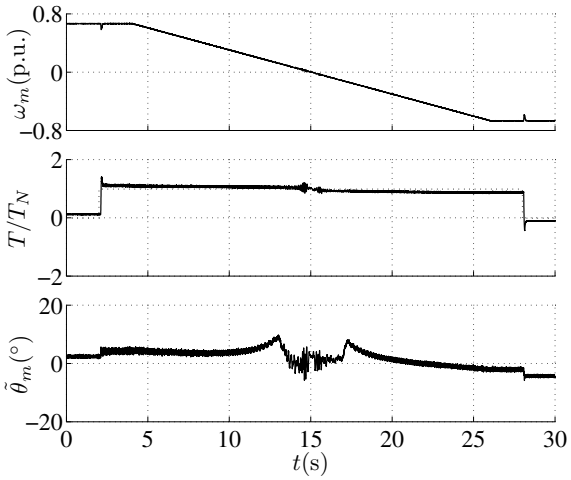


Fig. 8. Experimental results showing slow speed reversal at nominal load torque with speed-dependent gain. Explanations of the curves are as in Fig. 7.

speed follows the actual speed closely during fast changes in the electromagnetic torque. It can also be seen that the speed-dependent gain damps the vibrations more effectively than the constant gain. Moreover, the estimation error of the rotor position remains slightly smaller when using the speed-dependent gain. Persistent operation at zero speed under nominal load is possible due to the HF signal injection, which is in use at low speeds.

Fig. 8 shows experimental results from a slow speed reversal in the case of the speed-dependent gain. The load torque was kept at the nominal value between $t$ = 2 s and $t$ = 28 s, and the speed reference was changed from 0.67 p.u. to $-0.67$ p.u. between $t$ = 4 s and $t$ = 26 s. The estimated rotor speed follows the actual speed smoothly in the whole speed range in both motoring and regenerating modes. The noise is rejected effectively, and the estimation error of the rotor position is small even when a nominal load torque step is applied. The effect of the HF signal injection can be seen at low speeds; the estimation error of the rotor position increases with decreasing speed, but decreases rapidly when signal injection is taken into use at $\hat{\omega}_m = 0.13$ p.u. The ripple shown at low speeds is related to the HF signal injection method, which is sensitive to inverter nonlinearities and errors in measured phase currents.

## VI. Conclusions

The rotor speed and position of a permanent magnet synchronous motor can be estimated in a wide speed range, including zero speed, by means of an adaptive observer that is augmented with an HF signal injection technique at low speeds. The dynamic properties of the adaptive observer with different observer gains and in varying operating conditions were investigated using a linearized model derived for the motor and observer. According to the analysis, poor damping at high speeds can be avoided by selecting a speed-dependent feedback gain for the observer. The experimental results are in agreement with the results of the analysis. The adaptive observer together with the HF signal injection can cope with

stepwise changes in the speed reference and load torque, and the speed-dependent feedback gain improves the capability of damping unwanted vibrations and noise.

## APPENDIX

## CURRENT ERROR LINEARIZATION

The stator current derivative based on (1) and (2) is

$$\begin{aligned}\dot{\mathbf{i}}_s = {} & \mathbf{L}^{-1}\mathbf{u}_s - R_s\mathbf{L}^{-1}\mathbf{i}_s \\ & - \omega_m\mathbf{L}^{-1}\mathbf{J}\mathbf{L}\mathbf{i}_s - \omega_m\mathbf{L}^{-1}\mathbf{J}\boldsymbol{\psi}_{pm}\end{aligned} \tag{22}$$

The stator current transformed from the true rotor reference frame to the estimated rotor reference frame is

$$\mathbf{i}'_s = \mathbf{T}\mathbf{i}_s \tag{23}$$

where $\mathbf{T} = \cos\tilde{\theta}_m\mathbf{I} + \sin\tilde{\theta}_m\mathbf{J}$ is a coordinate transformation matrix, $\tilde{\theta}_m = \theta_m - \hat{\theta}_m$ being the rotor position error. Combining (22) and (23) gives the current dynamics in the estimated rotor reference frame

$$\begin{aligned}\dot{\mathbf{i}}'_s = {} & \tilde{\omega}_m\mathbf{J}\mathbf{i}'_s - R_s\mathbf{T}\mathbf{L}^{-1}\mathbf{T}^{-1}\mathbf{i}'_s \\ & - \omega_m\mathbf{T}\mathbf{L}^{-1}\mathbf{J}\mathbf{L}\mathbf{T}^{-1}\mathbf{i}'_s \\ & - \omega_m\mathbf{T}\mathbf{L}^{-1}\mathbf{J}\boldsymbol{\psi}_{pm} + \mathbf{T}\mathbf{L}^{-1}\mathbf{T}^{-1}\mathbf{u}'_s\end{aligned} \tag{24}$$

where $\tilde{\omega}_m = \omega_m - \hat{\omega}_m$ is the rotor speed error and $\mathbf{u}'_s = \mathbf{T}\mathbf{u}_s$. Linearizing this equation results in

$$\begin{aligned}\dot{\mathbf{i}}'_s = {} & (-R_s\mathbf{L}^{-1} - \omega_{m0}\mathbf{L}^{-1}\mathbf{J}\mathbf{L})\mathbf{i}'_s \\ & + \mathbf{J}\mathbf{i}_{s0}\tilde{\omega}_m + (-\mathbf{L}^{-1}\mathbf{J}\mathbf{L}\mathbf{i}_{s0} - \mathbf{L}^{-1}\mathbf{J}\boldsymbol{\psi}_{pm})\omega_m \\ & + (R_s\mathbf{L}^{-1}\mathbf{J}\mathbf{i}_{s0} - R_s\mathbf{J}\mathbf{L}^{-1}\mathbf{i}_{s0} \\ & \quad + \omega_{m0}\mathbf{L}^{-1}\mathbf{J}\mathbf{L}\mathbf{J}\mathbf{i}_{s0} - \omega_{m0}\mathbf{J}\mathbf{L}^{-1}\mathbf{J}\mathbf{L}\mathbf{i}_{s0} \\ & \quad - \omega_{m0}\mathbf{J}\mathbf{L}^{-1}\mathbf{J}\boldsymbol{\psi}_{pm} - \mathbf{L}^{-1}\mathbf{J}\mathbf{u}_{s0} + \mathbf{J}\mathbf{L}^{-1}\mathbf{u}_{s0})\tilde{\theta}_m \\ & + \mathbf{L}^{-1}\mathbf{u}'_s\end{aligned} \tag{25}$$

The adaptive model (5) of the observer is rewritten in terms of the the estimated current (6):

$$\begin{aligned}\dot{\hat{\mathbf{i}}}_s = {} & -R_s\mathbf{L}^{-1}\hat{\mathbf{i}}_s - \hat{\omega}_m\mathbf{L}^{-1}\mathbf{J}\mathbf{L}\hat{\mathbf{i}}_s \\ & - \hat{\omega}_m\mathbf{L}^{-1}\mathbf{J}\boldsymbol{\psi}_{pm} + \mathbf{L}^{-1}\mathbf{u}'_s + \mathbf{L}^{-1}\boldsymbol{\lambda}\tilde{\mathbf{i}}_s\end{aligned} \tag{26}$$

Linearizing and simplifying yields

$$\begin{aligned}\dot{\tilde{\mathbf{i}}}_s = {} & (-R_s\mathbf{L}^{-1} - \hat{\omega}_m\mathbf{L}^{-1}\mathbf{J}\mathbf{L} - \mathbf{L}^{-1}\boldsymbol{\lambda})\hat{\mathbf{i}}_s \\ & + (-\mathbf{L}^{-1}\mathbf{J}\mathbf{L}\mathbf{i}_{s0} - \mathbf{L}^{-1}\mathbf{J}\boldsymbol{\psi}_{pm})\hat{\omega}_m \\ & + \mathbf{L}^{-1}\boldsymbol{\lambda}\mathbf{i}'_s + \mathbf{L}^{-1}\mathbf{u}'_s\end{aligned} \tag{27}$$

Finally, the linearized equation of the current error $\tilde{\mathbf{i}}_s = \mathbf{i}'_s - \hat{\mathbf{i}}_s$ is obtained by subtracting (27) from (25) and substituting

$$\mathbf{u}_{s0} = R_s\mathbf{i}_{s0} + \omega_{m0}\mathbf{J}\mathbf{L}\mathbf{i}_{s0} + \omega_{m0}\mathbf{J}\boldsymbol{\psi}_{pm} \tag{28}$$

for the operating-point voltage. The result is

$$\begin{aligned}\dot{\tilde{\mathbf{i}}}_s = {} & (-R_s\mathbf{L}^{-1} - \omega_{m0}\mathbf{L}^{-1}\mathbf{J}\mathbf{L} - \mathbf{L}^{-1}\boldsymbol{\lambda})\tilde{\mathbf{i}}_s \\ & + (\mathbf{J}\mathbf{i}_{s0} - \mathbf{L}^{-1}\mathbf{J}\mathbf{L}\mathbf{i}_{s0} - \mathbf{L}^{-1}\mathbf{J}\boldsymbol{\psi}_{pm})\tilde{\omega}_m \\ & + (\omega_{m0}\mathbf{L}^{-1}\mathbf{J}\mathbf{L}\mathbf{J}\mathbf{i}_{s0} + \omega_{m0}\mathbf{i}_{s0} + \omega_{m0}\mathbf{L}^{-1}\boldsymbol{\psi}_{pm})\tilde{\theta}_m\end{aligned} \tag{29}$$


## ACKNOWLEDGEMENT

The authors gratefully acknowledge the financial support given by ABB Oy.


## REFERENCES


[1] R. Wu and G. R. Slemon, "A permanent magnet motor drive without a shaft sensor," *IEEE Trans. Ind. Applicat.*, vol. 27, no. 5, pp. 1005–1011, Sept./Oct. 1991.

[2] R. B. Sepe and J. H. Lang, "Real-time observer-based (adaptive) control of a permanent-magnet synchronous motor without mechanical sensors," *IEEE Trans. Ind. Applicat.*, vol. 28, no. 6, pp. 1345–1352, Nov./Dec 1992.

[3] S. Bolognani, R. Oboe, and M. Zigliotto, "Sensorless full-digital PMSM drive with EKF estimation of speed and rotor position," *IEEE Trans. Ind. Electron.*, vol. 46, no. 1, pp. 184–191, Feb. 1999.

[4] P. L. Jansen and R. D. Lorenz, "Transducerless position and velocity estimation in induction and salient AC machines," *IEEE Trans. Ind. Applicat.*, vol. 31, no. 2, pp. 240–247, March/April 1995.

[5] M. Linke, R. Kennel, and J. Holtz, "Sensorless position control of permanent magnet synchronous machines without limitation at zero speed," in *Proc. IEEE IECON'02*, vol. 1, Sevilla, Spain, Nov. 2002, pp. 674–679.

[6] E. Robeischl, M. Schroedl, and M. Krammer, "Position-sensorless biaxial position control with industrial PM motor drives based on INFORM- and back EMF model," in *Proc. IEEE IECON'02*, vol. 1, Sevilla, Spain, Nov. 2002, pp. 668–673.

[7] M. Tursini, R. Petrella, and F. Parasiliti, "Sensorless control of an IPM synchronous motor for city-scooter applications," in *Conf. Rec. IEEE-IAS Annu. Meeting*, vol. 3, Salt Lake City, UT, Oct. 2003, pp. 1472–1479.

[8] A. Piippo, M. Hinkkanen, and J. Luomi, "Sensorless control of PMSM drives using a combination of voltage model and HF signal injection," in *Conf. Rec. IEEE-IAS Annu. Meeting*, vol. 2, Seattle, WA, Oct. 2004, pp. 964–970.

[9] A. Piippo and J. Luomi, "Adaptive observer combined with HF signal injection for sensorless control of PMSM drives," in *Proc. IEEE IEMDC'05*, San Antonio, TX, May 2005, pp. 674–681.

[10] H. Kubota, K. Matsuse, and T. Nakano, "DSP-based speed adaptive flux observer of induction motor," *IEEE Trans. Ind. Applicat.*, vol. 29, no. 2, pp. 344–348, March/April 1993.

[11] G. D. Andreescu, "Position and speed sensorless control of PMSM drives based on adaptive observer," in *Proc. EPE'99*, Lausanne, Switzerland, Sept. 1999, CD-ROM.

[12] M. Hinkkanen, "Analysis and design of full-order flux observers for sensorless induction motors," *IEEE Trans. Ind. Electron.*, vol. 51, no. 5, pp. 1033–1040, Oct. 2004.

[13] T. Jahns, G. Kliman, and T. Neumann, "Interior permanent-magnet synchronous motors for adjustable-speed drives," *IEEE Trans. Ind. Applicat.*, vol. 22, no. 4, pp. 738–747, July/Aug. 1986.

[14] J. K. Pedersen, F. Blaabjerg, J. W. Jensen, and P. Thogersen, "An ideal PWM-VSI inverter with feedforward and feedback compensation," in *Proc. EPE'93*, vol. 5, Brighton, UK, Sept. 1993, pp. 501–507.